K.P. Geigle, M. Köhler, W. O'Loughlin, W. Meier, Investigation of soot formation in pressurized swirl flames by laser measurements of temperature, flame structures and soot concentrations, Proc. Combust. Inst. 35 (2015) 3373-3380.

The original publication is available at www.elsevier.com

http://dx.doi.org/10.1016/j.proci.2014.05.135

Investigation of soot formation in pressurized swirl flames by laser measurements of temperature, flame structures and soot concentrations

Klaus Peter Geigle*, Markus Köhler, William O'Loughlin, Wolfgang Meier

Deutsches Zentrum für Luft- und Raumfahrt e.V.
Institut für Verbrennungstechnik
Pfaffenwaldring 38-40
D-70569 Stuttgart (Germany)
* klauspeter.geigle@dlr.de
Tel. +49-711-6862 398
Fax +49-711-6862 578

Colloquium: Gas Turbines (IC Engine and Gas Turbine Combustion)
First alternate colloquium: Soot
Second alternate colloquium: Diagnostics

Abstract

Soot formation and oxidation were investigated in swirl flames operated with ethylene/air at elevated pressure in a gas turbine model combustor with optical access. Coherent anti-Stokes Raman scattering was used for temperature measurements, laser-induced incandescence for soot concentration and laser-induced fluorescence for the determination of OH radical distributions. A major focus of the experiments was the investigation of the influence of the injection of secondary oxidation air into the fuel-rich product gas of the primary combustion zone. Soot is mainly present in tiny filament-like regions left without OH signal. In the 3 bar flame with oxidation air injection these are found in a region separating the primary combustion zone, fed by combustion air and ethylene, and the secondary combustion induced by oxidation air and unburned hydrocarbons (UHC) that are transported into the inner recirculation zone. The different behavior of flames with and without oxidation air is most pronounced in the inner recirculation zone that is strongly influenced by the oxidation air admixture. This is reflected by changed OH distributions, mean temperatures and the shape of the temperature pdfs and results in significantly different soot distributions. The combined temperature statistics and correlated OH and soot distributions acquired at 3 and 5 bar are well suited to support the understanding of soot formation and oxidation and are expected to be a valuable input to soot model validation.

Key words: gas turbine, soot, CARS, pressure, LII/LIF

1. Introduction

Considerable effort has been expended to better understand and model soot formation in technical combustion, but reliable prediction of soot formation by numerical models is still far away. There has been reasonable progress in describing sub-processes present in simple or idealized flames such as premixed laminar or diffusion flames at atmospheric or increased pressure. However, adding technical features like turbulence, swirl or flame lift-off increases the complexity both experimentally and computationally. Experimental characterization of turbulent sooting flames either focuses on sub-processes [1,2], or quickly becomes too complex to serve for model validation. Very complex technical cases like fully-technical or industrial combustors [3], are rather used to monitor the overall behavior. Modeling of such cases is possible [4] but frequently lacks sufficient knowledge about the boundary conditions. There exists only a small number of data sets describing atmospheric jet flames with validation-data-quality and significant soot formation [5-7]. Suitable experiments to bridge the gap towards technical combustion are highly demanded. Measurements of soot concentrations and further quantities in gas turbine relevant flames have been performed, for example, by Lammel et al. [8] and Meyer et al. [9]. However, the results from those experiments are of limited amount or the combustor is too complex for model validation.

The current work aims at validation measurements under well-defined boundary conditions in a technically relevant gas turbine model combustor, exhibiting features such as swirl in combination with strong turbulence and increased pressure. Swirl stabilization in technical combustors as well as in the studied model combustor induces pronounced recirculation zones transporting hot exhaust gases and radicals upstream towards the injector. For the application of laser-based measurement techniques the combustor is equipped with large quartz windows. The investigations are motivated by the objectives of aircraft manufacturers to develop low-emission aero-engines. However, in order to limit the complexity with respect to numerical simulation, gaseous fuel (C_2H_4) was used instead of kerosene in this study, as in the validation cases mentioned above. One important feature of aero-engines is the oxidative influence of either cooling air injection or a second, lean combustion stage, for example [10]. Therefore our burner configuration enables injection of oxidation air downstream of the primary combustion zone. Temperature measurements in a similar burner described by Lammel et al. [8] demonstrated the cooling effect of this oxidation air which was partly convected far upstream by the swirl-induced recirculation. Recent soot concentration measurements by laser-induced incandescence [11] showed a clear influence of the oxidation air on the soot distribution in the flame core.

The new experiments focus on this influence by means of temperature distributions measured by coherent anti-Stokes Raman scattering (CARS) in combination with measurements of OH and soot distributions. Local temperature is one of the most important parameters influencing soot chemistry [12,13] and its spatially and temporally resolved measurement is of great value for the validation of soot models. In sooting flames, laser-based temperature measurements are problematic due to the presence of particles and large concentrations of aromatic compounds. One of the few techniques that perform reliably under such conditions is CARS in the version of shifted-vibrational CARS [14].

2. Experimental Setup

2.1 Burner

The burner is similar to the one used by Geigle et al. [15] and is described in a previous paper about quantitative soot measurements [11]. It consists of three concentric nozzles. Air at room temperature is supplied to the flame through a central (diameter 12.3 mm) and an annular nozzle (inner diameter 14.4 mm, outer diameter 19.8 mm). The air flows are fed from separate plenums and pass radial swirlers consisting of 8 channels (width w=4.2 mm, height h=5.4 mm, swirl number S=0.82 and swirl angle α_m=40.5° following the calculation in [16]) for the central nozzle and 12 channels (w=3.2 mm, h=4.5 mm, S=0.79, α_m=38.6°) for the annular nozzle. Gaseous fuel (C_2H_4) is injected in between both air flows through 60 straight channels (0.5×0.4 mm^2) forming a concentric ring. This fuel placement mimics the atomizing lip between swirled air flows as used for spray flames. The exit planes of the fuel and air nozzles are located at the level of the combustion chamber inlet, defined as height h=0. This allows full optical access to the fuel injection, in contrast to previous experiments [8,15]. The combustion chamber measures 120 mm in height and has a square section of 68×68 mm^2 with beveled edges (see Fig. 1). Four 3-mm-thick quartz windows (127×59 mm^2) are mounted between four water-cooled metal posts yielding excellent optical access of 51.4×120 mm^2 to the flame. The water-cooled top plate has a cylindrical exhaust hole (diameter 40 mm, length 24 mm), linked to the combustion chamber by a curvature. The high velocity in the exhaust tube prevents any backflow from outside the combustion chamber. Each of the corner posts has an additional air duct of 5 mm diameter for the injection of secondary air into the combustor at a height of 80 mm. The four radially-injected jets meet on the combustor axis and form a stagnation point. A metal plate shields the burner

front plate from the hot combustion gases during operation. This is required because of the lack of external cooling of this part.

The combustor is mounted in a water-cooled steel pressure housing with large optical access (60×120 mm^2) from 4 sides. The pressure can be adjusted by partially blocking the exhaust port with a movable piston. An air flow through the gap between the combustion chamber and the pressure housing serves as air cooling for the windows of the combustion chamber. The inner surface of the combustor windows does not show any degradation during operation, but exhibits some soot deposition at certain operating conditions. The surface temperature is estimated to be between 500 and 900 °C, depending on the position relative to the location of the flame. For modeling purposes, the quartz window transmission curves can serve to estimate the radiative energy balance.

The combustor was designed for operation at approximately 10 kW/bar thermal power providing Re numbers clearly above 10000 [11]. The flow rates for the different operating conditions are shown in Table 1. The air and fuel flows were controlled using electronic mass flow controllers (Bronkhorst) which were carefully calibrated in-house; the accuracy of the calibration is estimated to be below 1% of the maximum flow rates. The equivalence ratio ϕ and thermal power P were calculated from the primary air flow rate Q_{air} as a sum of central ($Q_{air,c}$) and ring air ($Q_{air,r}$), whereas the global equivalence ratio ϕ_{global} and the global thermal power P_{global} were calculated from the total air flow rate, $Q_{air}+Q_{oxi}$. The amount of oxidation air is given as fraction Q_{oxi}/Q_{air}. Note that due to the excess fuel the value for P is limited by the combustion air mass flow in most cases whereas ϕ_{global} becomes lean after injection of oxidation air and thus P_{global} depends on the fuel mass flow. The air split ratio is defined as the ratio of central air to the total combustion air $Q_{air,c}/Q_{air}$. For this ratio a value of 0.3 is chosen. For higher values the sooting region shifts towards the flame periphery, leading to increased soot deposition on the inner surface of the combustion chamber windows.

From previous measurements in a similar combustor it is known that the flow field consists of a conically shaped inflow region with relatively high flow velocities, an inner and an outer recirculation zone and the shear layers between the inflow and the recirculating flows [15].

For the current study a subset of operating points was selected from those presented in [11]. Parameters that have a strong influence on soot formation are pressure (studied at 3 and 5 bar) and oxidation air (with/without), which defines the selected flames presented here (see Table 1).

2.2 Optical Setup

2.2.1 Laser-induced incandescence (LII) and laser-induced fluorescence (LIF)

For the simultaneous acquisition of LII and LIF images 2 different lasers are used for excitation. For LII, the fundamental of a Nd:YAG laser (Brilliant B, Quantel) at λ=1064 nm is formed into a homogeneous light sheet by a cylindrical (f=-50 mm) and a spherical lens (f=1000 mm). An approximately 47 mm tall laser sheet of 0.3 mm thickness is created in the measurement plane using a rectangular aperture. The clipped region exhibits a relatively uniform fluence of 0.4 mJ/cm^2 ± 15%. The corresponding pulse energy of 55 mJ is set by attenuating the laser beam with a half wave plate and polarizer combination.

LII images are recorded perpendicular to the excitation plane with an image-intensified dual frame CCD camera (DicamPro, PCO) equipped with a Nikon f/2.5 camera lens. The first exposure of 60 ns duration serves to acquire the flame luminosity background immediately before the laser pulse while the second frame captures the first 60 ns of the LII signal.

For excitation of OH fluorescence, a dye laser (Sirah PRSC-G-24-EG) was pumped by the second harmonic of a Nd:YAG laser (Spectra Physics PIV-400-10). After frequency doubling, pulse energies of approximately 5 mJ at 283 nm were used for OH excitation. The beam was expanded into a sheet of 90 mm height and 0.4 mm waist thickness in the measurement location by using a cylindrical (f=-50 mm) and a spherical lens (f=750 mm). OH molecules were excited using the $Q_1(8)$ line of the $A^2\Sigma$-$X^2\Pi$ (1,0) transition at λ=283.55 nm, the exact wavelength tuning was validated in a reference burner. Shortly before entering the combustor this sheet was combined with the IR sheet by a UV mirror transmitting 1064 nm radiation.

The fluorescence signal emitted at 90° is separated from LII by a UV mirror, collected by an achromatic UV lens (Cerco, Sodern 100 mm) and detected by an intensified CCD camera (Imager Pro Plus, LaVision). For OH PLIF measurements a gate duration of 200 ns and a band pass filter around 315 nm were employed (Hugo Anders) to reduce background signal. OH LIF images were corrected for CCD chip sensitivity and laser sheet inhomogeneities. For beam profile correction, part of the laser sheet was deflected into a quartz cell filled with fluorescent dye solution (Coumarin 120 in ethanol) and simultaneously imaged by an additional CCD camera (Imager Pro X, LaVision). Timing of the fluorescence experiment relative to LII was such that the UV beam crossed the flame 400 ns before the IR beam to prevent interference between the two measurement systems while still having a short enough delay that the measurements are effectively simultaneous. Only images with LII excitation in the lower laser sheet position are included in the discussion below. The determination of the

quantitative time-averaged soot distributions has been described recently [11], while the instantaneous LII images presented here, acquired simultaneously with OH distributions, did not require calibration for the purpose of this study.

2.2.2 Coherent anti-Stokes Raman Scattering (CARS)

For the temperature measurements, broadband N_2 vibrational CARS was applied in a folded BOXCARS configuration [14,17]. The 532 nm radiation of a Nd:YAG laser (GCR230, Spectra Physics, pulse duration ≈8 ns) operated at 10 Hz was used to pump a customized dye laser system (Precision Scan, Sirah), composed of one narrowband (λ=582 nm) and one broadband (λ≈685 nm) dye laser. By shifting the excitation wavelengths away from 532 nm, CARS signal interferences with laser-induced C_2 emissions were avoided [14]. The energy of each beam was independently controlled by attenuators composed of a half-wave plate and a polarizer. The pulse energies used depended on the N_2 density at the measurement location and were in the range of 4–13 mJ for the broadband beam and 9–27 mJ for the narrowband beam. Behind the attenuator, the narrowband beam was split in two and the three laser beams were then focused by a spherical lens (f=250 mm) into the combustion chamber. In the overlapping focal region of the three beams the CARS signal was generated and emitted as a coherent beam. After recollimation, the CARS signal was separated from the laser beams by an aperture and two dichroic mirrors, and subsequently focused into a fiber (UV400, Avantes). The signal was dispersed by a double-grating spectrograph (Model 1403, Spex) and recorded by an iCCD camera (Flamestar 2F, LaVision). From a measurement without flame, the spatial resolution was found to be L95% = 1.6 mm with a diameter of the probe volume of approximately 300 μm. Parallel polarization was used to gain maximum signal strength in this demanding technical burner layout. For evaluation of the CARS signal, a temperature dependent local gas concentration deduced from equilibrium calculations is taken into account reducing the otherwise resulting large uncertainty of the temperature significantly.

The lowest accessible measurement location in the flame was at 0.7 mm above the burner surface. In the flame without oxidation air, the windows were partly covered by soot deposits. These were removed by the laser beams for CARS excitation. An additional IR laser was used to keep the position of the CARS signal on the combustor exit window clear of soot deposits. Radial temperature profiles were typically measured in one half of the flames only. For the flame with oxidation air a control point was added on the opposite side of the flame for each radial profile to confirm flame symmetry and consistency of the measurements.

CARS measurements in these flames turned out to be challenging. Beam steering due to thermal gradients influenced the beam overlap and thus the signal levels. In some locations strong local temperature fluctuations led to a high dynamic intensity range of the signals resulting in events of detector saturation or low signal levels. Those locations were measured a second time with lower excitation laser energy to capture the initially saturated signals; combination of the resulting temperature information was done in post-processing. Data analysis followed that presented by Lückerath et al. [18]. Not all single-shot CARS spectra could be analyzed for each measurement location. In the data analysis it was verified that exclusion of corrupt single spectra did not lead to a bias of the resulting temperature distributions. In unclear cases certain measurement positions were excluded from analysis.

3. Results and Discussion

3.1 Soot and OH distributions

One key question arising from the soot measurements by LII in the flames studied in [11] regards the influence of the oxidation air radially injected downstream of the main or primary combustion zone. A comparison of the time-averaged soot distributions without and with oxidation air is displayed in Fig. 2a and 2d. The LII measurements for the 3 bar flame with oxidation air, Fig. 2d, reveal that the oxidation air influenced the soot distribution significantly upstream of the injection location. While the flame without oxidation air, Fig. 2a, exhibited a relatively broad soot distribution, the injection of oxidation air resulted in a hollow soot distribution at lower soot concentration levels. The corresponding time-averaged OH PLIF images reveal more detail about this influence. Without oxidation air (Fig. 2b) the V-shaped OH distribution known from similar gas turbine model, or technical combustors ([19,20] and references therein) encloses the downstream portion of the fresh-gas inflow, contoured by the dashed line on the left side, and represents the (primary) flame zone. Further downstream, in the inner recirculation zone, OH levels are low. Soot (Fig. 2a) is on average mainly present near the centerline in the region surrounded by the OH distribution and at moderate concentrations outside of the OH distribution in the region of the outer recirculation zone, (ORZ). For the respective flame with oxidation air (Fig. 2c), significant additional OH signal is observed in the inner recirculation zone. However, there exists a weak separation between the OH formed from the oxidation air and that formed in the primary combustion zone, observable more clearly in the instantaneous distribution shown and discussed in Fig. 3c below. The bottom part of the OH distributions of both flames looks quite

similar in shape, while the intensity is higher in the case with oxidation air (Fig. 2b). Further downstream, close to the burner axis, OH signal levels decrease.

Further details can be seen in the instantaneous distributions in Fig. 3. The fresh-gas inflow is visible at the bottom of the LIF images b and c, representing the flame without and with oxidation air, respectively, as the region without OH. The high OH LIF signals observed in the images are indicative of super-equilibrium OH concentrations which are present in and close to the reaction zones. In the inner recirculation zone in Fig. 3b low OH levels are observed which indicate the presence of hot gas close to chemical equilibrium.

Figs. 3c and 3d show the influence of oxidation air on a single shot basis for the 3 bar flames in simultaneously recorded OH PLIF/LII image pairs. With oxidation air, wrinkled OH structures fill a large part of the combustion chamber including the whole inner recirculation zone with a gap towards the primary flame zone. As visible in the corresponding LII image (Fig.3c and 3d), this gap correlates to a soot layer (right branch of the flame). However, the gap seen on the left side in the OH PLIF image does not match with any soot filament in the LII image and might be filled with unburned hydrocarbon species or soot precursors not yet grown to soot. In the inner recirculation zone, IRZ, oxidation air reacts with unburned hydrocarbons that survived the primary flame zone and generates “secondary” OH. The respective flame without oxidation air is characterized by soot filaments adjacent to the OH distribution in the inner recirculation zone (Fig. 3a and 3b). Here, soot presence is not confined by OH clouds in the flame center, as in the flame with oxidation air, and thus can fill up the whole inner recirculation zone, leading to the continuous soot distribution shown in Fig. 2a. In both cases, overlap of soot and OH is minor.

At 5 bar the separation region between primary and secondary combustion visible in the time-averaged OH distribution is more distinct, and its correlation to soot existence is more pronounced (Fig. 4). Soot is mostly present in the region above the primary flame zone where mean OH concentrations are low. No soot is detected in the central IRZ downstream of 45 mm above the burner surface, equal to the respective 3 bar flame.

3.2 Temperature distributions

At each location, typically 1200 single shot CARS measurements were performed from which the temperature pdfs were deduced. Fig. 5 shows axial profiles of the mean temperatures, the widths σ of the pdf distributions, and the correlated soot volume fractions. σ is determined based on a Gaussian distribution fitted to the

measured histogram (see Fig.6). The conditions at h=3 mm are characterized by cold temperature, negligible fluctuations and soot concentrations, i.e. unreacted gas. This is in agreement with the observation that the flame is lifted by a few millimeters. High temperatures at 12 mm coincide with soot levels close to maximum. The location of the gradient corresponds to the stagnation point between inflow and the reverse flow in the inner recirculation zone, and soot present here was most probably formed on the fluid passage through the IRZ that provides the necessary residence times. Downstream, the mean temperature levels off at about 2000 K for the flame without oxidation air, i.e. approx. 400 K below the adiabatic flame temperature T(ad) for the global equivalence ratio of this flame. With oxidation air this profile changes remarkably. The temperature decrease due to admixture of cold air extends from h≈40 mm to h>110 mm and is strongest at the height of oxidation air injection, correlated with the absence of soot. For h<40 mm the temperature level of the flame with oxidation air (3 bar) is higher than that of the corresponding flame without oxidation air. The temperature increase is probably due to the partial burnout of the fuel-rich combustion products from the primary combustion zone. The significant mean soot concentrations in the same region are explained by occasionally occurring soot build-up. A pressure increase to 5 bar correlates with a more pronounced soot formation by roughly a factor of 4 (Fig. 5, compare Figs. 2 and 4). The resulting increased radiative loss is probably responsible for a reduction of the mean temperatures in the lower IRZ.

A more detailed characterization is given by the temperature histograms, a selection of which are displayed in Fig. 6. Parameters of fitting a Gaussian distribution (T(mean) and σ, used in Fig. 5) as well as most probable temperature T(mp), 90% temperature range and number of analyzed spectra are included. Fig. 7 displays radial profiles of T(mp) and temperature fluctuations at h=3 and 18 mm for the 3 bar flame without oxidation air. As a measure of the width of the distribution the bars in this plot show the range in which 90% of all measured temperatures lie for a given location, because Gaussian fits and the parameter σ are not reasonable in the shear layer region. This region is of particular importance for the stabilization of the studied flames, and gas turbine flames in general because here the recirculating hot gas from the IRZ (and partly from the ORZ) collides with the inflowing fresh fuel/air mixture and ignites it [21]. The unsteady nature of the shear layer becomes obvious from the steep gradients of the axial and radial temperature profiles and the increased temperature fluctuations. The radial profile at h=3 mm shows a transition from the cold inflow (r≤8 mm) towards the hot outer recirculation zone (r=16 mm) with large fluctuations in the shear layer between them (r=12 mm) where the temperatures vary between 600 and 2000 K (corresponding histograms shown in Fig. 6a

to 6c). Soot is present a the outer radial locations at this height, while no soot formation or transport is seen in the cold or fluctuating zone (compare to the mean soot distribution in Fig. 2a). The radial profile at h=18 mm in Fig. 7 shows T(mp)=1900 K (equal to mean temperature here) close to the flame axis and an increasing probability of low temperatures with increasing radius. The wide, homogeneously populated temperature range for r=12 - 20 mm corresponds to the mixing region of fresh inflow and recirculated exhaust gases leading to ignition and combustion of fresh gases. There exist no instantaneous temperatures beyond T(ad) neither here nor in the inner recirculation zone. The IRZ is characterized by a quite homogeneous temperature field exhibiting a narrow distribution with σ typically around 80 K (well represented by Fig. 6d). Towards the stagnation point the mean temperature decreases moderately while the distribution widens.

For the respective flame with oxidation air a very similar general behavior for the inflow region was observed (not shown). However, temperatures in the ORZ are lower by ≈200 K. The most pronounced differences compared to the flame without oxidation air occur in the inner recirculation zone. In general, the distributions are significantly broader as seen in the histograms in Fig. 6d and 6e, both on axis at the height of oxidation air injection. Instantaneous temperatures exceed those measured in the flame without oxidation air, and on the flame axis even 2400 K is measured (Fig. 6f). This indicates a significant contribution of the oxidation air to the local mixture, leading temporally to almost stoichiometric combustion. The mixture conditions in the central region of the combustor are thus frequently unfavorable for soot formation. The combination of instantaneous OH distribution and temperature histograms provides a consistent explanation for the differences of the soot distributions in both flames. For the flames with oxidation air soot is mainly formed in the boundary between the primary flame and the secondary combustion in the IRZ supplied by the additional oxidation air. Further downstream, in regions without significant soot presence, the temperature profile and temperature histograms of the 5 and 3 bar flames with oxidation air become very similar (not shown). Both local temperature and local equivalence ratio contribute to soot concentrations. Without knowledge of the latter the effect of temperature cannot easily be identified. Nevertheless, the provided accurate temperature data and statistics are expected to be an essential parameter for soot model validation and in combination with those might provide insight into radiative losses that were not measured experimentally.

4. Conclusions

A swirl-stabilized gas turbine model combustor with optical access was used to study soot formation and oxidation at gas turbine relevant conditions and to provide validation data for numerical simulations. Flames with and without additional oxidation air were studied by planar laser-induced fluorescence of OH, planar laser-induced incandescence for soot concentrations and coherent anti-Stokes Raman scattering for temperature determination. As expected, significant differences were observed between the flames with and without oxidation air injection. While the flames behaved similarly in the primary combustion zones, significant differences occurred downstream of this region. The OH distributions revealed large areas of secondary combustion caused by the mixing of fuel-rich combustion gases from the primary zone with secondary air. Consequently, the soot concentration levels were much lower than in the flame without oxidation air. The strong fluctuations of the mixing and reaction progress were well captured by the single shot CARS measurements. The temperature pdfs exhibited quite different shapes in different areas of the flames: The regions of the inflow and the exhaust gas were characterized by narrow distributions at low and high temperatures, respectively. In the shear layers, bimodal distributions were measured reflecting the intermittent occurrence of cold gas from the inflow and hot gas from the recirculation zones. In the region where secondary air was mixed with combustion products, the distributions were broad but mostly mono-modal. The results from the various measurement techniques are consistent in themselves and reflect the physical and chemical processes in the flame. The combined results from these measurements present a new and comprehensive data set for the validation of numerical simulations. Local equivalence ratio and temperature are strongly linked; the determined temperatures thus are not suited to explain differences between the studied flames, yet shall be valuable to model validation. Particle image velocimetry (PIV) measurements are planned to complement the data set by providing the velocity fields of the cold and reactive flows.

Acknowledgement

Part of this work was funded by the European Commission within the project Fuel Injector Research for Sustainable Transport (FIRST) under contract no. 265848.

References

[1] V.R. Katta, R.A. Forlines, W.M. Roquemore, W.S. Anderson, J. Zelina, J.R. Gord, S.D. Stouffer, S. Roy, Combust. Flame 158 (2011) 511–524.

[2] V. Narayanaswamy, N.T. Clemens, Proc. Combust. Inst. 34 (2013) 1455–1463.

[3] U. Meier, S. Freitag, J. Heinze, L. Lange, E. Magens, M. Schroll, C. Willert, C. Hassa, I. K. Bagchi, W. Lazik, M. Whiteman, J. Eng. Gas Turbines Power 135(2013), 121508.

[4] T. Blacha, M. Di Domenico, P. Gerlinger, GT2011-45084, Proc. ASME Turbo Expo 2011, Vancouver, Canada

[5] S. Lee, S.R. Turns, R.J. Santoro, Combust. Flame 156 (2009) 2264-2275.

[6] J. Zhang, C.R. Shaddix, R.W. Schefer, Rev. Sci. Instrum. 82 (2011) 074101.

[7] M. Köhler, K.P. Geigle, T. Blacha, P. Gerlinger, W. Meier, Combust. Flame 159 (2012) 2620-2635.

[8] O. Lammel, K.P. Geigle, R. Lückerath, W. Meier, M. Aigner, GT2007-27902, Proc. ASME Turbo Expo 2007, Montreal (Canada).

[9] T.R. Meyer, S. Roy, V.M. Belovich, E. Corporan, J.R. Gord, Appl. Opt. 44 (2005) 445-454.

[10] M. Carl, T. Behrendt, C. Fleing, M. Frodermann, J. Heinze, C. Hassa, U.E. Meier, D. Wolff-Gaßmann, S. Hohmann, N. Zarzalis, J. Eng. Gas Turbines Power 123 (2001) 810-816.

[11] K.P. Geigle, R. Hadef, W. Meier, J. Eng. Gas Turbines Power 136, 021505 (2013).

[12] H. Bockhorn, Soot Formation in Combustion, Springer Verlag, Berlin-Heidelberg-New York, 1994, p. 149 ff.

[13] H. Jander N. Petereit, D.M. Razus, Z. Phys. Chem. 188, 159-175 (1995).

[14] K.P. Geigle, Y. Schneider-Kühnle, M.S. Tsurikov, R. Hadef, R. Lückerath, V. Krüger, W. Stricker, M. Aigner, Proc. Combust. Inst. 30 (2005) 1645-1653.

[15] K.P. Geigle, J. Zerbs, M. Köhler, M. Stöhr, W. Meier, J. Eng. Gas Turbines Power 133 (2011) 121503.

[16] D. Galley, S. Ducruix, F. Lacas, D. Veynante, Combust. Flame 158 (2011) 155–171.

[17] M. Köhler, K.P. Geigle, W. Meier, B.M. Crosland, K.A. Thomson, G.J. Smallwood, Appl. Phys. B 104 (2) (2011) 409-425.

[18] R. Lückerath, M. Woyde, W. Meier, W. Stricker, U. Schnell, H.C. Magel, J. Görres, H. Spliethoff, H. Maier, Appl. Opt. 34 (1995) 3303–3312.

[19] W. Meier, I. Boxx, M. Stöhr, C.D. Carter, Exp. Fluids 49 (2010) 865-882.

[20] U. Stopper, W. Meier, R. Sadanandan, M. Stöhr, M. Aigner, G. Bulat, Combust. Flame 160 (2013) 2103-2118.

[21] R. Weber, J. Dugué, Prog. Energy Combust. Sci. 18 (1992) 349–367.

Tables

Table 1. Flame parameters for studied flames: Pressure, p, flow rates for air through burner (central and ring), $Q_{air,c}$, and $Q_{air,r}$, fuel, Q_{fuel}, oxidation air through secondary air inlet, Q_{oxi}, equivalence ratios, ϕ, ϕ_{global}, thermal powers, P, P_{global}, and fractions $Q_{air,c}/Q_{air}$ and Q_{oxi}/Q_{air} with $Q_{air}=Q_{air,c}+Q_{air,r}$. Flow rates in standard liters per minute (slm) are referenced to 1.013 bar and 273 K.

p [bar]	ϕ	$P_{primary}$ [kW]	$Q_{air,c}$ [slm]	$Q_{air,r}$ [slm]	Q_{fuel} [slm]	Q_{oxi} [slm]	$\frac{Q_{air,c}}{Q_{air}}$	$\frac{Q_{oxi}}{Q_{air}}$	ϕ_{global}	P_{global} [kW]
3	1.2	32.2	140.8	328.5	39.3	0	0.3	0	1.2	32.2
3	1.2	32.2	140.8	328.5	39.3	187.4	0.3	0.4	0.86	38.6
5	1.2	53.7	234.2	546.2	65.4	312.1	0.3	0.4	0.86	64.4

Figures – Caption List

Fig. 1: Burner geometry, nozzle details and cross section at the height of oxidation air injection, with the laser sheet and CARS measurement positions introduced.

Fig. 2: Time-averaged soot and OH distributions for the 3 bar rich flames without (left) and with oxidation air (right), CARS measurement points labelled, those selected for Fig. 6 are bold. The dashed line in image b) indicates the fresh gas inflow. LII images measure 60.4 x 113.8 mm^2, OH images 54 x 77 mm^2.

Fig. 3: Instantaneous distributions corresponding to the plots in Fig. 2.

Fig. 4: Time-averaged soot and OH distributions for 5 bar rich flame with oxidation air.

Fig. 5: Vertical profiles including mean temperatures and the width of distribution (bars). The dashed lines indicate adiabatic flame temperatures for the combustible mixture with and without inclusion of oxidation air. At the bottom the corresponding soot profiles are shown.

Fig. 6: Some examples of representative temperature distributions at different locations in the flames; locations labelled bold in Fig. 2.

Fig. 7: Radial temperature profiles for the 3 bar flame without oxidation air including the most probable temperatures T(mp) and the range of 90% of measured temperatures at 3 and 18 mm above the burner surface.

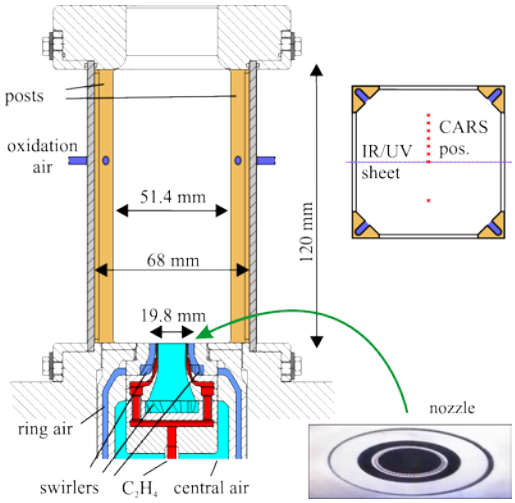

Fig. 1: Burner geometry, nozzle details and cross section at the height of oxidation air injection, with the laser sheet and CARS measurement positions introduced.

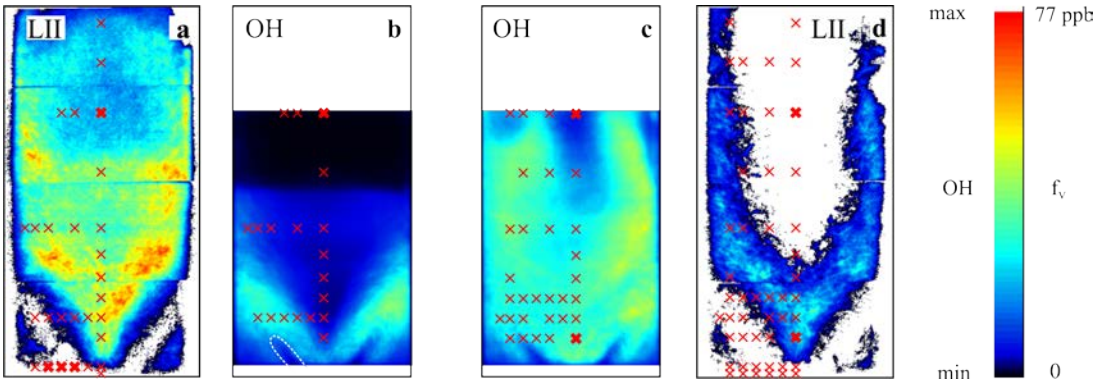

Fig. 2: Time-averaged soot and OH distributions for the 3 bar rich flames without (left) and with oxidation air (right), CARS measurement points labelled, those selected for Fig. 6 are bold. The dashed line in image b) indicates the fresh gas inflow. LII images measure 60.4 x 113.8 mm^2, OH images 54 x 77 mm^2.

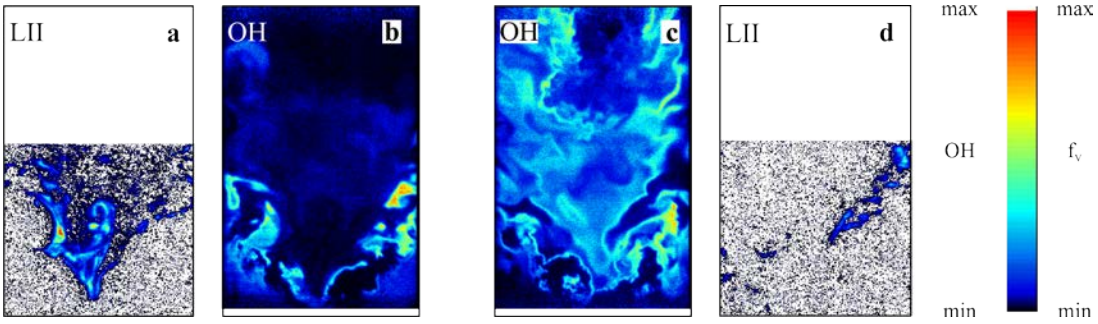

Fig. 3: Instantaneous distributions corresponding to the plots in Fig. 2.

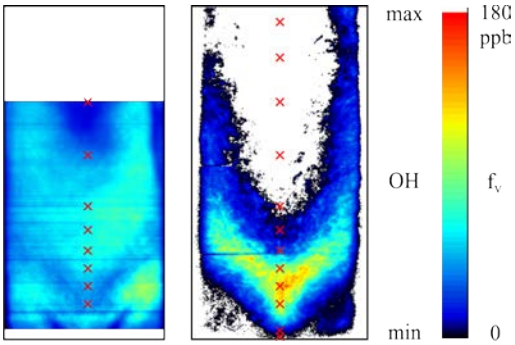

Fig. 4: Time-averaged soot and OH distributions for 5 bar rich flame with oxidation air.

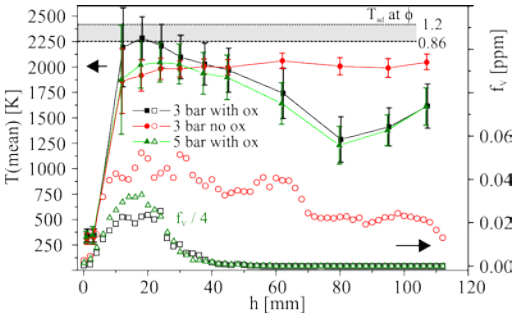

Fig. 5: Vertical profiles including mean temperatures and the width of distribution (bars). The dashed lines indicate adiabatic flame temperatures for the combustible mixture with and without inclusion of oxidation air. At the bottom the corresponding soot profiles are shown.

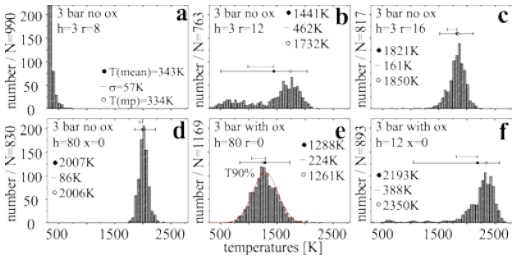

Fig. 6: Some examples of representative temperature distributions at different locations in the flames; locations labelled bold in Fig. 2.

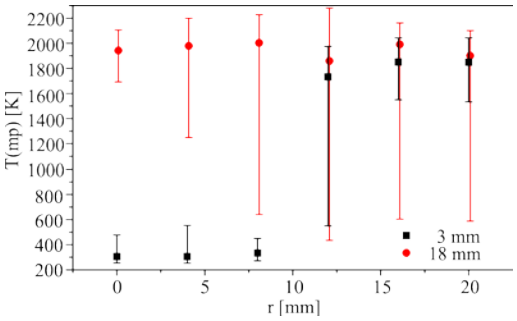

Fig. 7: Radial temperature profiles for the 3 bar flame without oxidation air including the most probable temperatures T(mp) and the range of 90% of measured temperatures at 3 and 18 mm above the burner surface.